Biocompatibility and Systemic Safety of a Novel Implantable Annuloplasty Ring for the Treatment of Mitral Regurgitation in a Minipig Model

Yuval Ramot, Serge D. Rousselle, Nadav Yellin, more...

Show all authors

First Published February 27, 2016 | Research Article | Check for updates

https://doi.org/10.1177/0192623315627217

Article information

Abstract

Prosthetic annuloplasty rings are a common treatment modality for mitral regurgitation, and recently, percutaneous implantation techniques have gained popularity due to their favorable safety profile. Although in common use, biocompatibility of annuloplasty rings has been reported only sparsely in the literature, and none of these reports used the percutaneous technique of implantation. We report on the biocompatibility and the systemic safety of a novel transcatheter mitral valve annuloplasty ring (AMEND™) in 6 minipigs. This device is composed of a nitinol tube surrounded by a braided polyethylene terephthalate fabric tube. The device produced no adverse inflammatory response, showing gradual integration between the metal ring and the fabric by normal host fibrocellular response, leading to complete neoendocardium coverage. There was no evidence for adverse reactions, rejection, or intolerance in the valvular structure. In 2 animals, hemopericardium resulted from the implantation procedure, leading to right-sided cardiac insufficiency with pulmonary edema and liver congestion.

Keywords

mitral regurgitation, safety studies, annuloplasty ring, percutaneous delivery, biocompatibility

Introduction

Mitral regurgitation (MR) is among the most common valvular heart diseases, with moderate to severe disease seen in up to 13.3% of patients older than 75 years of age (Nkomo et al. 2006). In functional MR (as opposed to degenerative MR), the mitral valve leaflets are anatomically normal, and the regurgitation can occur secondary to ischemia, nonischemic dilated cardiomyopathy, or both (Fukamachi 2008; Yacoub and Cohn 2004). Such conditions can lead to an imbalance between the closing and the tethering forces of the mitral valve, mitral annulus, and left ventricle wall (Gillam 2008; Karimov, Kobayashi, and Fukamachi 2012; Le and Thys 2006). With time, this disorder can progress to left ventricle dysfunction and congestive heart failure, resulting in high rates of reduced functional capacity and mortality and increased health-care costs (Agricola et al. 2009; Grasso et al. 2015).

The optimal treatment modality, its timing, and possible effectiveness are still debated (Atluri and Acker 2012; Borisenko et al. 2015; Raja and Berg 2007). Current guidelines recommend surgery for patients with left ventricle dysfunction associated with moderate-to-severe MR, and mitral valve repair is the preferred method of treatment (Nishimura et al. 2014). The most commonly used procedure is the placement of prosthetic annuloplasty rings to restore normal annular geometry and function (Witschey et al. 2015). Nevertheless, many of the patients with functional MR are over 75 years of age with additional comorbidities and suffer high operative mortality (Biancari et al. 2013). Therefore, these patients are often denied surgery and need to resort to isolated clinical management, which carries lower prognosis (Grasso et al. 2015). It is on this background that percutaneous techniques have emerged as an alternative treatment modality to MR. These techniques include

catheter, the system changes its geometrical configuration from a linear system to a close D-shape ring. After the deployment in the atrium is completed, the implant is anchored to the native annulus using a 4-zone mechanism. We aim to evaluate the biocompatibility and the systemic safety of this device in a minipig model.

Animals, Materials, and Methods

Test Device

The AMEND implant has three different sizes: small, medium, and large. The sizes differ in dimensions and quantity of anchors. In this study, we used the medium size in all 6 cases. The AMEND comprises a laser cut nitinol tube with an integrated nitinol sheet anchoring mechanism. The Ni-Ti tube shape is set to a D-shape ring, emulating the geometrical shape of the valve. Locking the distal and proximal ends of the ring to a close D-shape ring is done using a titanium locking mechanism (Figure 1).

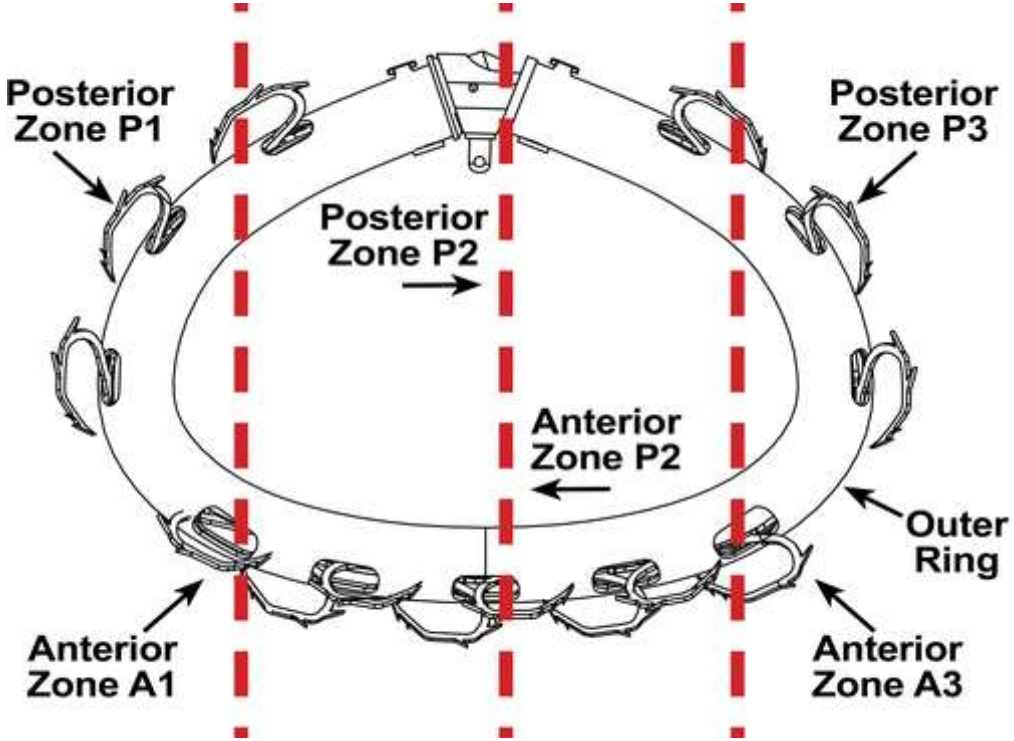

Figure 1. Scheme of the device. The 3 red dotted lines show the position of the three anteroposterior sections that were performed for histopathological evaluation.

Attachment of the ring to the mitral annulus is done with the help of the anchoring mechanism. This mechanism is divided into 4 zones of anchors around the ring with 2 zones in the posterior side and 2 zones in the anterior side (Figure 1). A laser cut extruded polyethyleneterephthalate (PET) tube (Zeus Industrial products, Inc., NJ, USA) is bonded with ultraviolet curing glue (Loctite # 3104) to the ring internal surface to avoid metal-to-metal contact and decrease friction between the ring internal diameter and the anchoring mechanism. In the medium size implant, the 2 posterior zones have 3 Ni-Ti anchors each and the 2 anterior zones have 4 nitinol anchors each; 14 anchors verify durable anchoring of the ring to the tissue (Figure 1).

Each of the 4 zones is activated separately from the delivery system handle. At activation, the anchors exit the ring, hooking the annulus tissue, thus fixating the ring to the annulus. The anchors' design includes harpoon-like

features to increase ring fixation. A laser cut braided PET fabric tube (Secant Medical, Inc., PA, USA) is sutured to the ring outer diameter using a 7-0 ultrahigh molecular weight polyethylene suture (Force fiber, Teleflex Inc., NC, USA). The purpose of the PET fabric is to promote the tissue ingrowth post implantation.

Implant selection and device sizing was done based on several criteria:

A. The commissure-to-commissure dimension of the annulus has to be equal or smaller than the commissure-to-commissure dimension of the ring (34 ± 1 mm). Thus, verifying good contact in the commissures area where no reduction is required.

B. The anterior–posterior dimension of the annulus has to be greater than the anterior–posterior dimension (24.5 ± 1 mm) of the ring to achieve reduction of the anterior–posterior dimension after implantation.

C. The atrium height has to be larger than 20 mm to provide enough working volume.

In this study, the medium size ring was selected, as it had the closest fit to the animals' annulus dimensions and corresponded to the sizing criteria. The annulus dimensions of the animals ranged between 30 and 36 mm in the commissure-to-commissure dimension and 25 and 28 mm in the posterior–anterior dimension.

Animals and Housing

Six female Sinclair minipigs were obtained from Ben Meir farm, Yokneam, Israel. This experiment was performed in accordance with the guidelines of the Israeli Institutional Animal Care and Use Committee (IACUC). The study was approved by the Israeli IACUC (permit number IL-14-10-281). All efforts were made to minimize animal suffering.

The minipig model was chosen for this study since it is an acceptable model for cardiovascular devices due to the corresponding anatomy of the cardiovascular system of the swine to the cardiovascular system of humans (Bode et al. 2010; Swindle et al. 2012).

Experimental Design

Before starting the procedure, general condition of the animals and vital signs were recorded. During the procedure, heparin was given as an anticoagulation to maintain the activated clotting time above 250 sec. For the implantation of the device, the animal was placed on its back, and a 12-Fr introducer sheath was inserted into the right femoral artery, allowing the placement of a high-flow pigtail catheter. The delivery system included a 36-Fr catheter with a distal handle that actuates the various mechanisms of the implant, for example, closure of the implant and anchoring to the tissue. The delivery of the implant was done via a transapical beating heart approach using a double purse ring on the access site in the apex.

Median sternotomy with opening of the pericardium was performed in order to allow access for epicardial echocardiography (EE). EE and quality images are considered essential to achieve successful and accurate implantation. The standard transesophagus echocardiography does not provide high-quality images in the swine model due to different anatomy (lungs are located between the esophagus and the heart) and relatively large esophagus. The EE probe was used to allocate the penetration point and mark it on the heart. Access point selection was performed in two axes—intracommissural and left ventricular outflow tract—therefore allowing the perpendicularity of the delivery system and the mitral valve plane during implantation. Angiography and echocardiography were used to visualize the catheter, implant, and mitral apparatus during the implantation procedure. The catheter was advanced through the left ventricle to the left atrium. Once positioned in the left atrium, the ring was emitted out of the catheter to form a D-shape geometry and a dedicated mechanism closed the distal and proximal ends of the ring. Once the ring configuration was ready, it was oriented in short and long axes and fixed to the annulus. The fixation of the ring to the annulus was done by anchoring the posterior zones first and sequentially the anterior zones. Following implantation, the animal chest was closed, and fluoroscopy was performed to verify implant stability and angiography to verify implant position. Three animals were sacrificed after 64 days, 1 animal after 75 days, and 2 animals after 109 days.

Necropsy and Tissue Handling

All animals were subjected to a complete necropsy evaluation by a board certified pathologist, which included the evaluation of the carcass and musculoskeletal system; all external surfaces and orifices; cranial cavity and

external surfaces of the brain; and thoracic, abdominal, and pelvic cavities with their associated organs and tissues. The following tissues were collected from all sacrificed animals: spleen, lungs, liver, and right kidneys. These tissues were embedded in paraffin, sectioned, mounted on glass slides, and stained with hematoxylin and eosin (H&E).

Hearts were harvested, rinsed with saline, saved intact, and fixed in 10% neutral buffered formalin for at least 72 hr post necropsy. Each heart was trimmed above and below the mitral annulus to expose the device and all valves, including the mitral annuloplasty implant. In addition, the ventricular myocardium was breadloafed at regular intervals and examined macroscopically. The annulus with implant and all portions of the heart were examined macroscopically, and any abnormalities were described and recorded. Particular attention was paid to dehiscence of the implant and any surface abnormalities as well as any possible downstream changes in the myocardium. The implant site (mitral valve) was photographed on both the atrial and ventricular sides, and, when present, gross abnormalities were also photographed. Each implant site was scored macroscopically for several criteria including thrombus formation, structural integrity (tears), neoendocardium formation and calcification, using a predefined scoring system, and a diagram depicting the distribution of observations of interest, as applicable (Supplementary Material).

The explanted annulus with implant was radiographed at 2 perpendicular incidences using a Faxitron X-ray cabinet and high-resolution film. The radiographs were digitized and assessed for any abnormalities (namely, structural integrity of the implant and calcification). The implant site was dehydrated and cleared and infiltrated in Epon (Spurr), following an extended schedule befitting the implant size. Any gross lesions found in the heart and not directly associated with the implant site were trimmed, photographed, and processed to slide in paraffin. The plastic blocks containing the implant site were sectioned using an Exakt diamond band saw along 3 parallel antero-posterior planes as illustrated in Figure 1. Care was taken to properly orient the resulting wafer specimen with markers for anterior/posterior side (A/P) and zone (1, 2, or 3). Section 2 (A2–P2) was very slightly off-center to avoid the very center of the snap mechanism. Additional slides (gross lesions at the implant site not captured in routine sections) were trimmed at the designated levels, and the resulting plastic wafers were mounted to

properly labeled slides, ground, and micropolished to microscopic finish. All slides (all plastic slides and any paraffin slides) were stained with H&E.

Histopathology Examination

The parameters, which were assessed and recorded to evaluate the biological response to the implanted device, were based on the international standards ISO 10993-6 (2007) and Ramot et al. (2015), including (but were not limited to) the presence and severity of thrombosis; presence and extent of neointima formation (~neoendocardium); neointima maturity based on fibro-cellular density and presence or absence of residual fibrin; presence and extent of endothelial coverage; presence of dehiscence and regurgitation channels at the annulus; tissue ingrowth within the polyester fabric; the presence and extent of fibrosis/fibrous capsule—neoendocardium (semiquantitative grading); the extent and severity of inflammation and types of inflammatory cells present within or around the capsule and within the polyester mesh; degeneration as determined by changes in tissue morphology; presence, extent, and type of necrosis; tissue alterations within the cavity of implantation such as fragmentation and/or debris presence, fatty infiltration, granuloma formation, and bone formation; presence and form of test device remnants, material fragmentation, and debris; and nature and extent of tissue ingrowth if applicable.

The scaling of the lesions was based on the semiquantitative criteria presented by Shackelford et al. (2002), in which grade 1 corresponds to lesion barely noticeable, and/or up to 10% of the tissue is affected; grade 2—the lesion is noticeable but is not a prominent feature of the tissue, and/or up to 20% of the tissue is affected; grade 3—the lesion is a prominent feature of the tissue and/or up to 40% of the tissue is affected; grade 4—the lesion is an overwhelming feature of the tissue, and/or more than 41% of the tissue is affected.

Results

Necropsy Findings

One animal from the 64-day sacrifice point had extensive hematoma in the subcutis, located along the lateral wall of the posterior part of the body. In addition, red-stained fluid filled the abdominal and thoracic cavity (total amount about 3 L). In the lungs, the anterior part of the lobes had a “hepatic”-like aspect. In 1 animal from the 109-day sacrifice point, a hematoma, forming a cyst-like structure of 2.5 cm in diameter, was found in the base of the left ventricle of the heart. In all the other 4 animals, no abnormality was detected as part of the necropsy examination.

Macroscopic Findings

64-day sacrifice time point

In all 3 animals, the heart showed fibrous adhesions between the epicardium and the pericardium diffusely (expected surgical healing reaction). The anterior apex showed an area of transmyocardial pale discoloration, ranging from 12–20 × 6–12 mm on cross sections, containing prolene suture material. This finding was consistent with the healed access site.

In 1 animal (i.e., the animal with the hematoma in the subcutis), there was a red nodule (~27 × 25 × 15 mm) within the epicardium over the anterior right ventricle. The left lateral pericardium also showed an area of tan discoloration and thickening. These changes were consistent with nonprogressive and organizing hematoma, likely dating from the surgical procedure and gradually resolving through fibrous organization. In another animal, there was an area of white discoloration in the myocardium of the left ventricle (~12 × 3 mm) that may be consistent with a fibrous scar, judged to be related to the operation procedure, and not due to the presence of the implanted ring. In the same animal, there was an area of pale discoloration on the endocardial surface of the left lateral atrium that was consistent with a “jet lesion” indicative of MR. The mitral valve in this animal showed a small defect in the posterior free edge of the lateral leaflet. This defect may have been the cause for regurgitation indirectly evidenced through the observation of a jet lesion in the left atrium. Except for this lesion, there were no structural abnormalities and deployment appeared nominal with no conformational changes of note; namely, the mitral valve appeared normal and showed regular coaptation as did all other heart valves. There was a thin layer of neoendocardium formation over most of the fabric cover of the implant, although some areas appeared yet

uncovered. The uncovered areas showed no thrombus deposition as stated above. No grossly visible thrombus formation or calcium deposits were detected.

75- and 109-day sacrifice time points

There were no gross abnormalities in the heart from these animals, except for 1 animal from the 109-day sacrifice time point, where a large nodule (~8 × 6 × 3 cm) extending from the base to the distal third of the ventricle toward the apex was seen in the left lateral aspect of the heart. Upon sectioning, the mass appeared filled with dark brown material consistent with coagulated blood. This lesion was interpreted macroscopically as a hemopericardium.

Macroscopic scoring data revealed no grossly visible thrombus formation or calcium deposits. There were no structural abnormalities and deployment appeared nominal with no conformational changes of note; namely, the mitral valve appeared normal and the leaflets showed regular coaptation as did all other heart valves. There was a thin layer of neoendocardium formation over the entire length of the fabric cover of the implant and good apposition through the circumference (Figure 2).

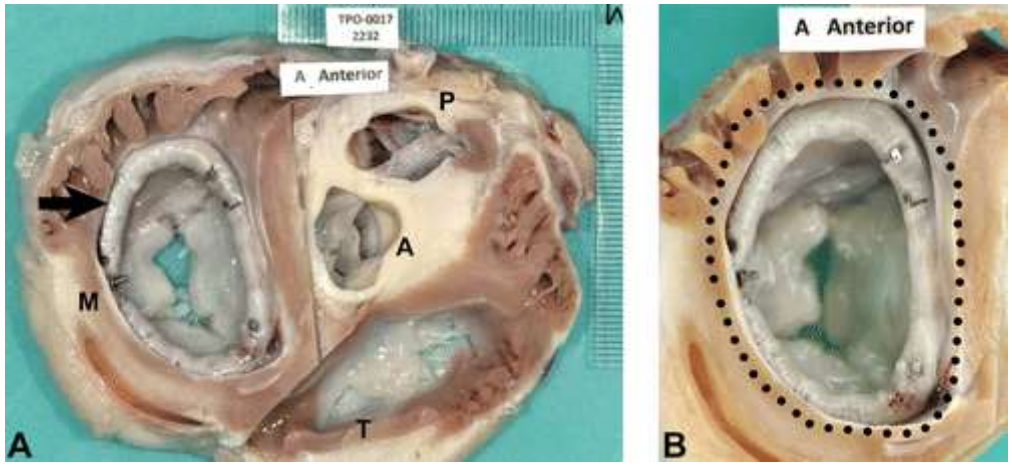

Figure 2. (A) Subgross aspect of the heart trimmed transversally at the level of the valves. Arrow indicates the implanted device. A = aorta; M = mitral valve; P = pulmonary artery; T = tricuspid valve. (B) Subgross aspect of

the annulus with the implant. The dotted line marks the fabric layer of the device, which is entirely covered by a glistening neoendocardium.

Radiographic Observations

In all animals, no conformational abnormalities were detected (Figure 3). The anchors appeared properly deployed in the surrounding tissue and showed no fractures. The surrounding tissue showed no evidence of calcification.

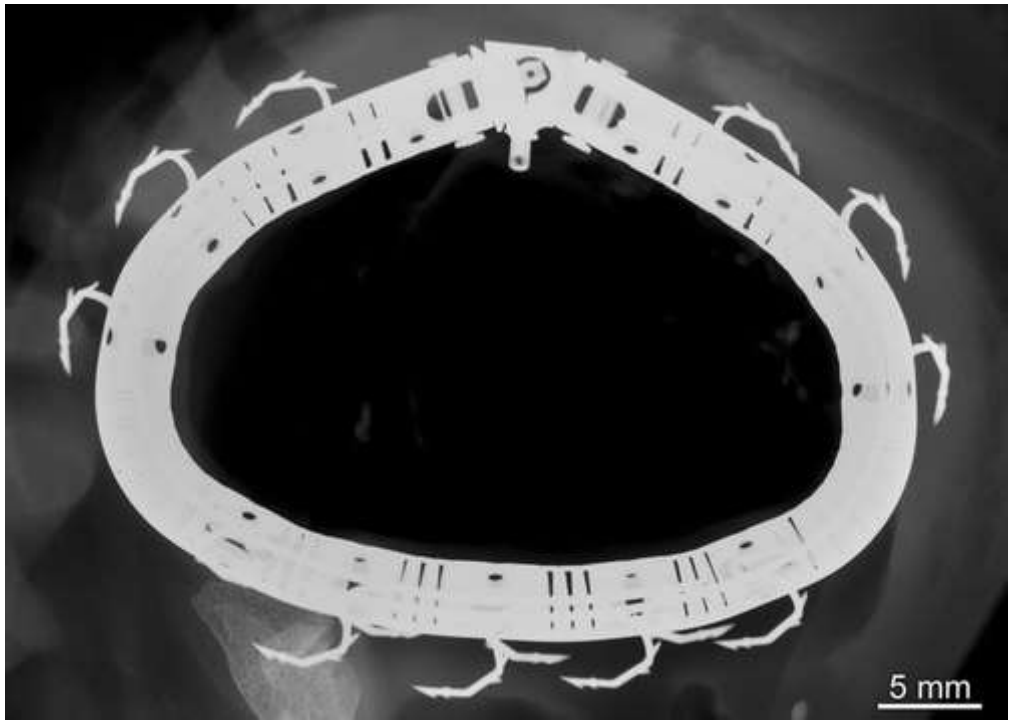

Figure 3. Full face X-ray of the mitral annular explant from an animal sacrificed at the 109-day time point, containing the annuloplasty device. There are no conformational abnormalities. The anchors appear properly deployed in the surrounding tissue and there are no fractures. The surrounding tissue does not show any evidence of mineralization.

Histopathology

Spleen, liver, kidney, and lungs

In 4 animals, no abnormalities were detected in the spleen, kidney, and lungs. Minimal inflammatory cell infiltration was seen in the liver, composed of mononuclear cells, characteristic of minor background changes.

In the animal from the 64-day sacrifice time point with the hematoma in the heart (see above), moderate centrilobular hepatocytic degeneration and necrosis and moderate centrilobular congestion were detected in the liver. This finding was accompanied with mild interstitial lymphocytic cell infiltration in the kidney and moderate lobar edema in the lung. In the animal with the hematoma from the 109-day sacrifice time point, mild inflammatory cell infiltration, composed of polymorphonuclear cells, indicative of an acute inflammatory reaction was seen in the liver. Additionally, mild sinusoidal dilation and congestion, associated with mild compressive atrophy of the hepatocytes, was seen. No other abnormalities were seen in other organs from this animal.

Heart

Overall, the entire surface of the ring was covered by the PET fabric tissue with only minor variations in coverage and was infiltrated by foreign body granulomatous reaction (absorbing the fabric; Figures 4–6). The intensity of the foreign body granulomatous reaction to the fabric was generally grade 2 in the interim sacrifice time point and was significantly decreased (i.e., generally grade 1) in the 75- and 109-day sacrifice time points. Neoendocardium, defined as soft tissue covering the device, was endothelialized, fibro-muscular, and well differentiated. Neoendocardium formation was graded mild at the early time point and moderate at the terminal sacrifice, and was seen around the ring nearly diffusely with only occasional small focal areas of no coverage noted. There was minor to mild collection of erythrocytes (hemorrhage) located between the fabric and the ring. The anchor was surrounded by neoendocardium formation with minimal to mild multifocal hemorrhage. In 1 case, minimal focal mineralization was seen.

Figure 4. Histology section at low magnification of implant site *in situ* within the heart trimmed transversally at the level of the mitral valve, showing cross section of the ring in anteroposterior plane. The photo is demonstrating that the device is appropriately deployed on the mitral annulus with no migration or dehiscence, indicating long-term stability of postoperative baseline conformation. Thick black arrows indicate the transversally sectioned ring. Thin arrow indicates native mitral leaflet. Dotted arrows indicate anchors visible beneath the rings. Arrowhead indicates the Os Cordis. Hematoxylin and eosin.

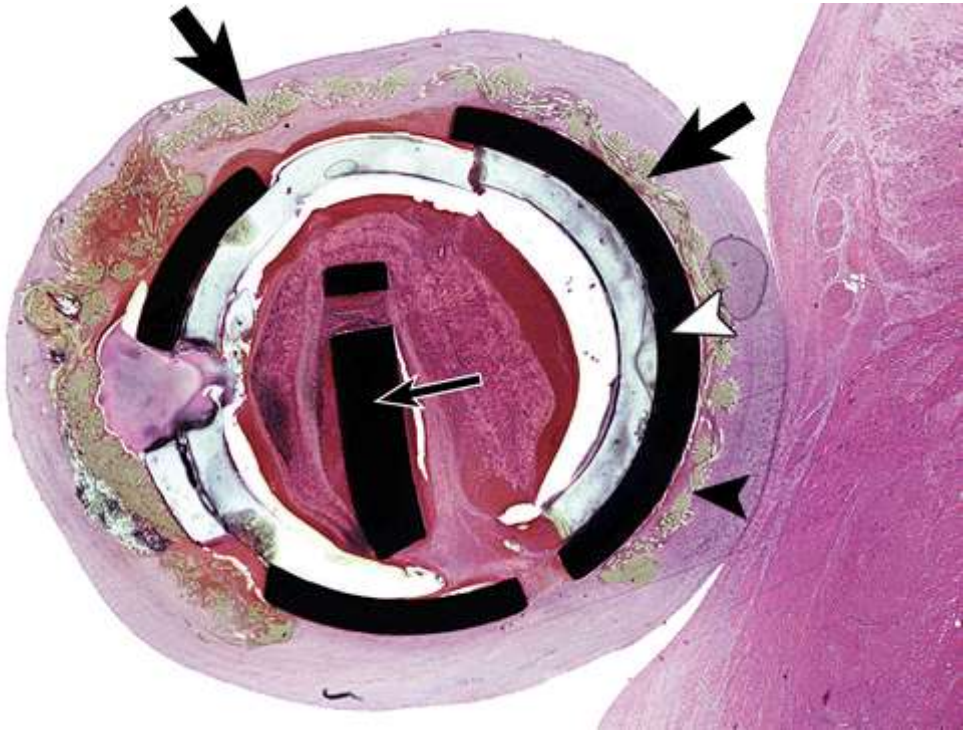

Figure 5. Higher magnification of the previous photo, showing a representative cross section of the ring in anteroposterior plane. The thick black arrows indicate the fabric located closely to the ring, which covers almost the entire circumference of the ring (white arrowhead). The fabric is embedded and entirely covered by neoendocardium (mature connective tissue). The black arrowhead indicates minimal collections of macrophages and giant cells, located closely to the fabric. Thin black arrow indicates cross section of the anchor assembly within the ring. The photo is demonstrating that structural integrity of the anchors and of the ring is maintained and that the ring is integrated within host tissue with no adverse response. Hematoxylin and eosin.

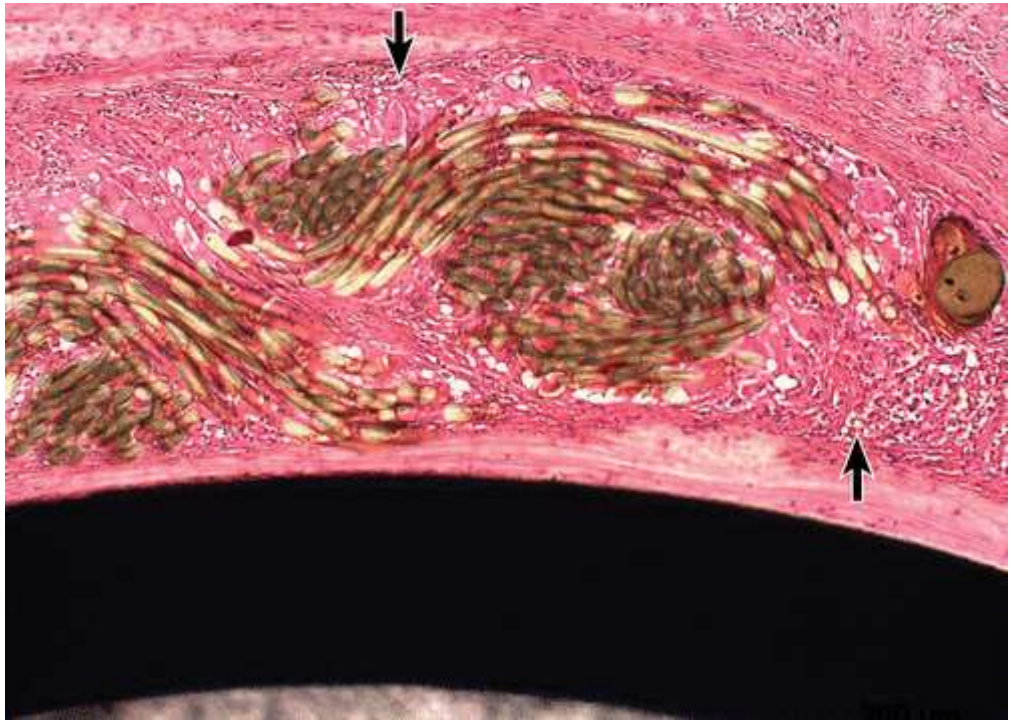

Figure 6. Higher magnification of the previous photo, showing a representative cross section of the ring in anteroposterior plane. The photo is demonstrating the minimal collections of macrophages and giant cells, located closely to the fabric (arrows). Hematoxylin and eosin.

Discussion

In this report, we described the biocompatibility and the systemic safety of a novel transcatheter mitral valve annuloplasty ring (AMEND). In all 6 animals, the fabric that covered the annuloplasty ring was embedded by minor foreign body granulomatous reaction. This reaction was surrounded by mature and endothelialized fibro-muscular connective tissue, consistent with neoendocardium. The grade of granulomatous reaction was intermediate at the 64-day time point, but tended to subside (i.e., minimally present), in the 109-day terminal sacrifice time point. The presence of time-related reduction in the intensity of the foreign body granulomatous

reaction toward the fabric is reported by Hagerty et al. (2000). The granulomatous response was limited to the immediate interface between the ring and the endocardium and did not spill over in the adjacent neoendocardium, annulus, or myocardium.

In all samples, the entire metal ring was covered by the organized neoendocardium, suggesting an excellent integration and/or anchoring of the metal ring to the adjacent cardiac tissue, via the formation of local endocardial capsular reaction. The penetration and complete involvement of the fabric by the connective tissue neoendocardium, without necrosis and/or mineralization, suggests an excellent coexistence and integration between the various components, without any evidence for adverse reaction, rejection, or intolerance in the valvular structure.

In 2 animals, hematomas were noted in the ventricular wall, judged to be related to the surgical procedure, and not due to the presence of the implanted rings. In these 2 animals, hepatic centrilobular congestion was evident, and in 1 animal, pulmonary edema was also seen. It is suggested that the animals primarily suffered from low-level, right-sided cardiac insufficiency resulting from the surgical access and coincidental hematoma formation, leading to compression of the right ventricle and secondary systemic chronic passive congestion.

The AMEND ring is composed of nitinol, which is the acronym for Nickel Titanium Naval Ordinance, an equiatomic nickel–titanium composition alloy (Shayan and Chun 2015). This alloy is in common use for endovascular devices (Barras and Myers 2000), including stents and vena cava filters. It is also widely used in valve prostheses (e.g., Corevalve™) and annuloplasty rings (e.g., Carpentier-Edwards Physio ring; Gourlay and Black 2010). Since a layer of titanium oxide is formed on its surface, preventing the diffusion of nickel atoms, nitinol is considered a biologically inert material (Shabalovskaya 2002). Nevertheless, it should be taken into consideration that thrombotic complications can occur when implanted in small arteries (Ramot and Nyska 2007; Ramot, Nyska, and Spectre 2013).

Several *in vivo* biocompatibility studies have shown in the past that the use of nitinol in endovascular devices led to the formation of normal neointima. Such was the case in an *in vivo* swine test, where thin film nitinol-covered stent was implanted in the external iliac artery, resulting in normal endothelialization without neointimal

hyperplasia or thrombosis (Tulloch et al. 2011). A similar reaction was observed after the implantation of a thin film nitinol flow diverter in swine arteries, again resulting in the growth of a thin layer of healthy neointima (Kealey et al. 2012). Our observations indeed underline the excellent tolerability of the nitinol ring, and in our case, no thrombotic complications were seen.

The nitinol tube in the AMEND device was covered by PET fabric, which is used commonly to replace damaged blood vessels and valves (Al Meslmani et al. 2015; Desai, Seifalian, and Hamilton 2011; Ozaki et al. 2014). Although in common use, PET has been reported previously as a trigger for chronic inflammation, characterized by the presence of activated macrophages, foreign body giant cells, and capsule formation, which can be the source for excessive tissue encapsulation (Hagerty et al. 2000; van Bilsen et al. 2004; Wang et al. 2010). However, in this study, the inflammation was minimal and tended to decrease overtime, and the PET covering led to the desirable formation of a mature and stable fibro-muscular neoendocardium.

Taking into consideration the fact that detailed reports on pathology reactions and biocompatibility of implanted annuloplasty rings in pigs are relatively sparse in the scientific literature, our report can serve as an example for normal and expected reactions to such devices. It can also help in understanding the normal reactions that can be anticipated due to access procedures and surgical trauma.

Based on the pathology observations, it can be concluded that the implanted device was optimally tolerated, leading to time-related integration between the metal ring, the fabric, and host endocardium, leading to formation of mature connective tissue neoendocardium coverage, without any evidence for adverse reaction, rejection, or intolerance in the valvular apparatus or adjacent myocardium.

Author Contribution

Authors contributed to conception or design (SR, NY, UW, IS, AA, AN); data acquisition, analysis, or interpretation (YR, SR, NY, AN); drafting the manuscript (YR, AN); and critically revising the manuscript (YR, SR, NY, UW, IS, AA, AN). All authors gave final approval and agreed to be accountable for all aspects of work in ensuring that questions relating to the accuracy or integrity of any part of the work are appropriately investigated and resolved.

Declaration of Conflicting Interests

The author(s) declared the following potential conflicts of interest with respect to the research, authorship, and/or publication of this article: Dr. Abraham Nyska and Dr. Serge Rouselle served as consultants to Valcare for the pathology section of the project. Mr. Yellin is an employee of Valcare.

Funding

The author(s) disclosed receipt of the following financial support for the research, authorship, and/or publication of this article: The study was funded by Valcare, Inc.

Supplemental Material

The online data supplements are available at http://tpx.sagepub.com/supplemental.

References

Agricola, E., Ielasi, A., Oppizzi, M., Faggiano, P., Ferri, L., Calabrese, A., Vizzardi, E., Alfieri, O., Margonato, A. (2009). Long-term prognosis of medically treated patients with functional mitral regurgitation and left ventricular dysfunction. Eur J Heart Fail 11, 581–87. Google Scholar, Crossref, Medline, ISI

Al Meslmani, B. M., Mahmoud, G. F., Sommer, F. O., Lohoff, M. D., Bakowsky, U. (2015). Multifunctional network-structured film coating for woven and knitted polyethylene terephthalate against cardiovascular graft-associated infections. Int J Pharm 485, 270–76. Google Scholar, Crossref, Medline, ISI

Atluri, P., Acker, M. A. (2012). Mitral valve surgery for dilated cardiomyopathy: Current status and future roles. Semin Thorac Cardiovasc Surg 24, 51–58. Google Scholar, Crossref, Medline

Barras, C. D., Myers, K. A. (2000). Nitinol—Its use in vascular surgery and other applications. Eur J Vasc Endovasc Surg 19, 564–69. Google Scholar, Crossref, Medline, ISI

Biancari, F., Schifano, P., Pighi, M., Vasques, F., Juvonen, T., Vinco, G. (2013). Pooled estimates of immediate and late outcome of mitral valve surgery in octogenarians: A meta-analysis and meta-regression. J Cardiothorac Vasc Anesth 27, 213–19. Google Scholar, Crossref, Medline, ISI

Bode, G., Clausing, P., Gervais, F., Loegsted, J., Luft, J., Nogues, V., Sims, J. (2010). The utility of the minipig as an

animal model in regulatory toxicology. J Pharmacol Toxicol Methods 62, 196–220. Google Scholar, Crossref, Medline, ISI

Borisenko, O., Haude, M., Hoppe, U. C., Siminiak, T., Lipiecki, J., Goldberg, S. L., Mehta, N., Bouknight, O. V., Bjessmo, S., Reuter, D. G. (2015). Cost-utility analysis of percutaneous mitral valve repair in inoperable patients with functional mitral regurgitation in German settings. BMC Cardiovasc Disord 15, 43. Google Scholar, Crossref, Medline, ISI

Della Barbera, M., Laborde, F., Thiene, G., Arata, V., Pettenazzo, E., Pasquino, E., Behr, L., Valente, M. (2005). Sovering annuloplasty rings: Experimental pathology in the sheep model. Cardiovasc Pathol 14, 96–103. Google Scholar, Crossref, Medline, ISI

Desai, M., Seifalian, A. M., Hamilton, G. (2011). Role of prosthetic conduits in coronary artery bypass grafting. Eur J Cardiothorac Surg 40, 394–98. Google Scholar, Medline, ISI

Fukamachi, K. (2008). Percutaneous and off-pump treatments for functional mitral regurgitation. J Artif Organs 11, 12–18. Google Scholar, Crossref, Medline, ISI

Gillam, L. D. (2008). Is it time to update the definition of functional mitral regurgitation? Structural changes in the mitral leaflets with left ventricular dysfunction. Circulation 118, 797–99. Google Scholar, Crossref, Medline, ISI

Gourlay, T., Black, R. A. (2010). Biomaterials and devices for the circulatory system. Cambridge, UK: Woodhead. Google Scholar, Crossref

Grasso, C., Capodanno, D., Tamburino, C., Ohno, Y. (2015). Current status and clinical development of transcatheter approaches for severe mitral regurgitation. Circ J 79, 1164–71. Google Scholar, Crossref, Medline, ISI

Hagerty, R. D., Salzmann, D. L., Kleinert, L. B., Williams, S. K. (2000). Cellular proliferation and macrophage populations associated with implanted expanded polytetrafluoroethylene and polyethyleneterephthalate. J Biomed Mater Res 49, 489–97. Google Scholar, Crossref, Medline, ISI

ISO 10993 Technical Committee (2007) International Organization for Standardization (ISO) ISO Products and Services ISO Store Web site. Accessed August 22, 2007. www.iso.org/iso/en/ISOOnline.frontpage. Google Scholar

Kalangos, A., Sierra, J., Vala, D., Cikirikcioglu, M., Walpoth, B., Orrit, X., Pomar, J., Mestres, C., Albanese, S., Jhurry, D. (2006). Annuloplasty for valve repair with a new biodegradable ring: An experimental study. J Heart Valve Dis 15, 783–90. Google Scholar, Medline, ISI

Karimov, J. H., Kobayashi, M., Fukamachi, K. (2012). Functional mitral regurgitation: Modern concepts for ventricular geometry reshaping. Expert Rev Med Devices 9, 131–38. Google Scholar, Crossref, Medline, ISI

Kealey, C. P., Chun, Y. J., Vinuela, F. E., Mohanchandra, K. P., Carman, G. P., Vinuela, F., Levi, D. S. (2012). In vitro and in vivo testing of a novel, hyperelastic thin film nitinol flow diversion stent. Journal of Biomedical Materials Research. Part B, Applied Biomaterials 100, 718–25. Google Scholar, Crossref, Medline, ISI

Le, H. C., Thys, D. M. (2006). Ischemic mitral regurgitation. Semin Cardiothorac Vasc Anesth 10, 73–77. Google Scholar, SAGE Journals

Nishimura, R. A., Otto, C. M., Bonow, R. O., Carabello, B. A., Erwin, J. P., Guyton, R. A., O'Gara, P. T., Ruiz, C. E., Skubas, N. J., Sorajja, P., Sundt, T. M., Thomas, J. D. (2014). 2014 AHA/ACC guideline for the management of patients with valvular heart disease: Executive summary: A report of the American College of Cardiology/American Heart Association Task Force on Practice Guidelines. J Am Coll Cardiol 63, 2438–88. Google Scholar, Crossref, Medline, ISI

Nkomo, V. T., Gardin, J. M., Skelton, T. N., Gottdiener, J. S., Scott, C. G., Enriquez-Sarano, M. (2006). Burden of valvular heart diseases: A population-based study. Lancet 368, 1005–11. Google Scholar, Crossref, Medline, ISI

Ozaki, S., Saito, A., Nakaminami, H., Ono, M., Noguchi, N., Motomura, N. (2014). Comprehensive evaluation of fibrin glue as a local drug-delivery system-efficacy and safety of sustained release of vancomycin by fibrin glue against local methicillin-resistant *Staphylococcus aureus* infection. J Artif Organs 17, 42–49. Google Scholar, Crossref, Medline, ISI

Raja, S. G., Berg, G. A. (2007). Moderate ischemic mitral regurgitation: To treat or not to treat? J Card Surg 22, 362–69. Google Scholar, Crossref, Medline, ISI

Ramot, Y., Nyska, A. (2007). Drug-induced thrombosis—Experimental, clinical, and mechanistic considerations. Toxicol Pathol 35, 208–25. Google Scholar, SAGE Journals, ISI

Ramot, Y., Nyska, A., Markovitz, E., Dekel, A., Klaiman, G., Haim Zada, M., Domb, A., Maronpot, R. R. (2015). Long-term local and systemic safety of poly(l-lactide-coepsilon-caprolactone) after subcutaneous and intraarticular implantation in rats. Toxicol Pathol 43, 1127–40. Google Scholar, SAGE Journals, ISI

Ramot, Y., Nyska, A., Spectre, G. (2013). Drug-induced thrombosis: An update. Drug Saf 36, 585–603. Google Scholar, Crossref, Medline, ISI

Shabalovskaya, S. A. (2002). Surface, corrosion and biocompatibility aspects of Nitinol as an implant material. Biomed

Mater Eng 12, 69–109. Google Scholar, Medline, ISI

Shackelford, C., Long, G., Wolf, J., Okerberg, C., Herbert, R. (2002). Qualitative and quantitative analysis of nonneoplastic lesions in toxicology studies. Toxicol Pathol 30, 93–96. Google Scholar, SAGE Journals, ISI

Shayan, M., Chun, Y. (2015). An overview of thin film nitinol endovascular devices. Acta Biomater 21, 20–34. Google Scholar, Crossref, Medline, ISI

Swindle, M. M., Makin, A., Herron, A. J., Clubb, F. J., Frazier, K. S. (2012). Swine as models in biomedical research and toxicology testing. Vet Pathol 49, 344–56. Google Scholar, SAGE Journals, ISI

Tulloch, A. W., Chun, Y., Levi, D. S., Mohanchandra, K. P., Carman, G. P., Lawrence, P. F., Rigberg, D. A. (2011). Super hydrophilic thin film nitinol demonstrates reduced platelet adhesion compared with commercially available endograft materials. The Journal of Surgical Research 171, 317–22. Google Scholar, Crossref, Medline, ISI

van Bilsen, P. H., Popa, E. R., Brouwer, L. A., Vincent, J., Taylor, C. E., de Leij, L. F., Hendriks, M., van Luyn, M. J. (2004). Ongoing foreign body reaction to subcutaneous implanted (heparin) modified Dacron in rats. J Biomed Mater Res A 68, 423–27. Google Scholar, Crossref, Medline, ISI

Wang, Q., McGoron, A. J., Pinchuk, L., Schoephoerster, R. T. (2010). A novel small animal model for biocompatibility assessment of polymeric materials for use in prosthetic heart valves. J Biomed Mater Res A 93, 442–53. Google Scholar, Medline, ISI

Witschey, W. R., Zhang, D., Contijoch, F., McGarvey, J. R., Lee, M., Takebayashi, S., Aoki, C., Han, Y., Han, J., Barker, A. J., Pilla, J. J., Gorman, R. C., Gorman, J. H.. (2015). The influence of mitral annuloplasty on left ventricular flow dynamics. Ann Thorac Surg 100, 114–21. Google Scholar, Crossref, Medline, ISI

Yacoub, M. H., Cohn, L. H. (2004). Novel approaches to cardiac valve repair: From structure to function: Part II. Circulation 109, 1064–72. Google Scholar, Crossref, Medline, ISI

View Abstract

Toxicologic Pathology

ISSN: 0192-6233

Online ISSN: 1533-1601